increasing CO_2 concentration indicates that the global abundance of CO_2 in the atmosphere is increasing either due to increase in CO_2 emission or imbalance between sources and sinks of CO_2. On the other hand, the observed stable CH_4 concentration indicates a decrease in emissions, which may have accelerated the global methane budget towards a steady state. The reason for the change is unclear. Dlugokencky *et al.*[13] believe that a major contributing factor was the break-up of the Soviet Union in 1991. Oil and gas production fell, and the industry became more efficient at plugging gas leaks from pipes and wells. They also noted that the methane emissions from the former Soviet Union dropped significantly throughout the 1990s due to lower fossil-fuel production. Based on current knowledge of the observed data, it is not possible to tell whether we are only observing a persistent but temporary pause in its increase or global levels of methane are likely to stabilize in the near future. However, to derive acceleration and deacceleration of global budget of these trace gasses, it is necessary to have continuous measurements for prolonged duration.

1. Farman, J. C., Gardiner, B. G. and Shanklin, J. D., Large losses of total ozone in Antarctica reveal seasonal ClO_xNO_x interaction. *Nature*, 1985, **315**, 207–210.
2. Solomon, S., Progress towards a quantitative understanding of Antarctic ozone depletion. *Nature*, 1990, **347**, 347–354.
3. Mukhopadhyay, S. K., Biswas, H., De, T. K., Sen, B. K., Sen, S. and Jana, T. K., Impact of Sundarban mangrove biosphere on the carbon dioxide and methane mixing ratios at the NE Coast of Bay of Bengal, India. *Atmos. Environ.*, 2002, **36**, 629–638.
4. Hansen, J. E., Sato, M., Lacis, A., Ruedy, R., Gegen, I. and Matthews, E., Climate forcing in the industrial era. *Proc. Natl. Acad. Sci. USA*, 1998, **95**, 12,753–12,758.
5. Lacis, A., Hansen, J., Lee, P., Mitchell, T. and Lebedeff, S., Greenhouse effect of trace gases 1970–1980. *Geophys. Res. Lett.*, 1981, **8**, 1035–1038.
6. Wang, W.-C., Yung, Y. L., Lacis, A. A., Mo, T. and Hansen, J. E., Greenhouse effects due to man-made perturbation of trace gases. *Science*, 1976, **194**, 685–690.
7. Jain, A. K., Briegleb, B. P., Minschwaner, K. and Wuebbles, D. J., Radiative forcing and global warming potentials of 39 greenhouse gases. *J. Geophys. Res.*, 2000, **105**, 20773–20790.
8. Intergovernmental Panel on Climate Change (IPCC), *Climate Change 2001: The Scientific Basis* (eds Houghton, J. T. *et al.*), Cambridge University Press, New York, 2001.
9. Keeling, C. D. and Whorf, T. P., Atmospheric CO_2 records from sites in the SIO air sampling network. In *Trends: A Compendium of Data on Global Change*, Carbon Dioxide Information Analysis Center, Oak Ridge National Laboratory, Oak Ridge, Tenn., 1998.
10. Lelieveld, J., Crutzen, P. and Dentener, F. J., Changing concentration, lifetime and climate forcing of atmospheric methane. *Tellus*, 1998, **B50**, 128–150.
11. Lelieveld, J. and Crutzen, P. J., Indirect chemical effects of methane on climate warming. *Nature*, 1992, **355**, 339–342.
12. Dlugokencky, E. J., Report on the global atmospheric methane increase of 1998. *Geophys. Res. Lett.*, 2001.
13. Dlugokencky, E. J., Houweling, S., Bruhwiler, L., Masarie, K. A., Lang, P. M., Miller, J. B. and Tans, P. P., Atmospheric methane levels off: Temporary pause or a new steady-state? *Geophys. Res. Lett.*, 2003, **30**, 1992.
14. Francey, R. J. *et al.*, *Baseline Atmospheric Program (Australia) 1993* (eds Francey, R. J., Dick, A. L. and Derek, N.), 1996, pp. 8–29.
15. Dlugokencky, E. J., Masarie, K. A., Tans, P. P., Conway, T. L. and Xiong, X., Is the amplitude of the methane seasonal cycle changing? *Atmos. Environ.*, 1997, **31**, 21–26.

ACKNOWLEDGEMENTS. We thank to the Director, NPL, New Delhi and Head, RASD, NPL for their encouragement. Thanks are also due to the NCAOR (Department of Ocean Development) and CSIR for logistic and financial assistance.

Received 27 September 2004; revised accepted 28 January 2005

Nondestructive evaluation of the Delhi iron pillar

Baldev Raj, P. Kalyanasundaram, T. Jayakumar*, C. Babu Rao, B. Venkataraman, U. Kamachi Mudali, A. Joseph, Anish Kumar and K. V. Rajkumar

Metallurgy and Materials Group, Indira Gandhi Centre for Atomic Research, Kalpakkam 603 102, India

We discuss results obtained on nondestructive evaluation of the Delhi iron pillar using various non-destructive techniques such as ultrasonics, impact echo, radiography, radiation gauging, X-ray fluorescence, *in situ* metallography and electrochemical analysis. The microstructural analysis of the ornamental portion of the pillar indicated the presence of forged structure in the main body of the pillar, whereas the top platform consists of microstructure similar to 'as cast structure'. Further, the radiation gauging, radiography, ultrasonics and impact echo testing indicated the presence of voids at different locations in the pillar. The large aspect ratio (axial to radial) of the voids indicated that the pillar could have been forged in the radial direction rather than in the axial direction. The passivation current density for the 'passive' rust scales of the pillar formed on the surface clearly indicated the protective nature of the oxide structure developed and its stability against corrosion.

ANCIENT and medieval India did its countrymen proud and made tremendous impact on the world scene through many spectacular achievements in iron and steel technology. The technology of iron in India culminated in major achievements during the period 2nd–6th century AD. An exemplary monument of the time is the Delhi iron pillar (late fourth to early fifth century AD) standing at Mehrauli village, near Qutab Minar, on the outskirts of Delhi. It is a wrought iron product about 7.375 m high, 41.6 cm in diameter at the bottom and 34 cm at the top. The top has an aesthetic ornamental struc-

*For correspondence. (e-mail: tjk@igcar.ernet.in)

ture. Estimated to weigh more than 6000 kg, it is believed to have been built by forge-welding pieces of wrought iron (Figure 1). The pillar bears testimony to the fact that iron workers were experts in cementing and forge-welding small pieces or segments of iron to shape such large objects – a technique that was uncommon to the western world in that era. To make the Delhi iron pillar, it is estimated that at least 200 furnaces (typical 40 kg capacity) would have operated in tandem, or the same set of furnaces would have been used repeatedly to produce iron of such consistent and acceptable quality[1]. The techniques, of heating individual pieces and forge-welding to make acceptable joints, speak of sound awareness of the concepts of materials engineering in designing and erecting the monument. The pillar, until about the end of the 19th century was the heaviest known piece of wrought iron in the world. The Delhi pillar has long evoked the admiration of antiquarians and curiosity of metallurgists, principally for its large size and excellent state of corrosion resistance. Contrary to the earlier speculation and belief, it is now known, based on metallurgical investigations, that the composition and the structure of the samples taken from different locations of this pillar, and of the sample in itself, are significantly inhomogeneous. The composition of the wrought iron used in the pillar shows such a wide fluctuation as C (0.03–0.28), Si (0.004–0.056), and P (0.114–0.48) (ref. 2). Composition of other elements also shows considerable variations and the slag phase is irregular in distribution.

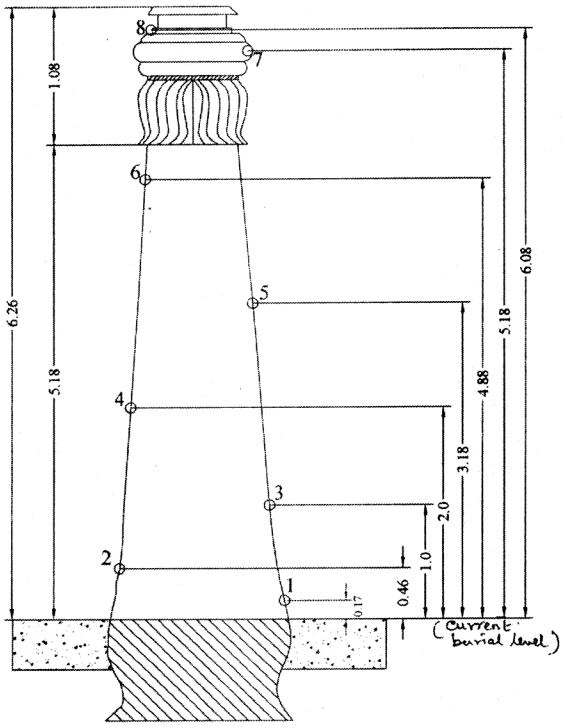

Figure 1. Schematic of the Delhi iron pillar showing the locations for metallography studies.

Scientific studies on the pillar were started by Hadfild, way back in 1912 (ref. 3). His studies were mainly focused around the dimensional measurements and chemical analysis of the samples taken from the pillar. Both western and Indian scientists have undertaken a number of investigations to probe the nature (composition, structure, etc.) of this fascinating monument.

Lal[4] carried out chemical analysis in 1945 and these values were quite close to those reported by Hadfield some 30 years back. In 1961 the pillar was dug out for chemical treatment and preservation, and then reinstalled by embedding the underground part in a newly constructed masonry pedestal. Following the excavation, a detailed examination of the entire pillar was carried out by Lal, and the measurements of different parts of the pillar were undertaken in detail. The state of the pillar in general and condition of the corroded and rusted areas in particular were photographically recorded. The overall weight of the pillar was found to be six tons.

Around 1963, Nijhawan took initiative for chemical, spectrochemical and electron probe analysis on a piece weighing about 4 g taken from the pillar. Although there were variations in the percentage of carbon, silicon and phosphorus, it was clear that the iron of the pillar is astonishingly pure, low in carbon, in particular, *vis-à-vis* the commercial varieties of today[5]. The latest investigations on the pillar were made in the year 1989 by Bindal *et al.*[6]. Pulse-echo technique of ultrasonic testing has been employed by Bindal *et al.* for microstructural characterization.

Studies of the iron pillar during the last thirty years, wherein Indian scientists and technologists could join hands effectively with their European counterparts, have thrown much light on the technology that went into the making of this massive monument well over 1500 years ago. The following facts have emerged from the earlier nondestructive, microscopic, X-ray, chemical and mechanical testing of this pillar by various researchers:

- The pillar iron is heterogeneous in composition and structure.
- The composition of the pillar iron is comparable to that of a low carbon steel.
- The visible weld lines, the marks due to strong hammering, the oxide film incorporating the slag and non-uniformity in composition strongly suggest that the pillar was forge welded quite ingeniously and effectively, starting with lumps of hot, pasty iron mixed with slag.
- There is no evidence of melting and subsequent solidification of the pillar iron, i.e. the pillar iron was never in liquid state.

No other aspect of the iron pillar has attracted such worldwide attention as the corrosion resistance of its cy-

lindrical exposed portion. Detailed scientific investigations have brought out several features of the pillar iron and its environment, each of which may have a bearing on the rustlessness associated with this ancient monument[7]. First, the low carbon iron of the pillar is characterized by high phosphorus, low sulphur, low manganese and high slag contents, apart from considerable inhomogeneity in the microstructure. All these features can contribute individually and collectively to good corrosion resistance in addition to the atmospheric factors. Secondly, the pillar is coated with a complex protective film varying in thickness from about 50 to 600 microns at different sections. The non-uniformity in microstructure characterized by slag inclusions, particularly at the grain boundaries, and structural imperfections such as slip bands and microstrains[8], is also likely to prevent intergranular corrosion and generally hinder progress of the corrosion process. Invoking the Mixed Potential Theory postulated in 1938 by Wagnar and Traud[9], Balasubramaniam[10,11] has suggested that the enhanced cathodic reactions due to the presence of slag particles at the grain boundaries can lead to the formation of passive protective film of phosphate, possibly in the glassy amorphous state conferring, thereby, high corrosion resistance to the pillar. The steps leading to formation of the protective film include (i) initial rust formation, (ii) increase in critical current density and the formation of the phosphate ($FePO_4$) on the matrix, and finally (iii) the extension of the phosphate film over the slag inclusions. The admirable corrosion resistance is attributed to the thin phosphate passive film on the pillar. Further, even though the microstructure of the main body of the pillar has been reported, the microstructural investigation of the decorative portion of the pillar has never been examined earlier.

The objective of the present study was to make a comprehensive evaluation of metallurgical technology employed for producing the iron with high corrosion resistance for centuries, the methodology adapted for building the iron pillar and to recommend suitable measures for its long term conservation. Even though a number of studies have been carried out on the pillar, a complete and comprehensive *in situ* assessment of the pillar using most modern nondestructive techniques has not been attempted. The advances in electronics, instrumentation and robotics have made it possible to have rugged and portable field units with higher sensitivity and accuracy. Thus, the objective of the present study is to carry out a wide variety of complementary NDE investigations and at a number of locations on the iron pillar so that comprehensive and statistical information could be obtained. Such a study could enhance the understanding of the ancient metallurgy and fabrication technologies adopted and also help in better understanding of the corrosion resistance of the iron pillar.

The NDE techniques chosen for investigation included ultrasonics, impact echo technique, radiography, radiation gauging, X-ray fluorescence, *in situ* metallography and electrochemical analysis. Of these, impact echo, radiography and radiation gauging are techniques which have not been attempted by any of the earlier workers. The results of the experimental campaign are presented and discussed for each technique in what follows.

The *in situ* metallography has been carried out on the pillar at eight different selected locations as indicated in Figure 1. Six of these locations lie on the main body (locations 1–6), one on the bell-shaped portion (location 7) and one on the top square platform (location 8). The *in situ* metallography studies indicated that the main body of the pillar (smooth surface section) has varying grain size with larger grains at the lower region (Figure 2 *a*) and smaller grains on the top region (Figure 2 *b*). Size and shape of the second phase present in the main body also varies from lower region to top regions. The inclusions are of needle-like nature at the lower region (Figure 2 *a*) and fine point in shape at the top region (Figure 2 *b*). The bell-shaped decorative region has fine-grained structure with second phase decoration along the grain boundaries (Figure 2 *c*).

The top square platform consists of microstructure similar to 'as cast structure' (Figure 2 *d*). However, almost similar microstructure has also been reported at one of the locations in a piece cut from the main portion of the pillar[5].

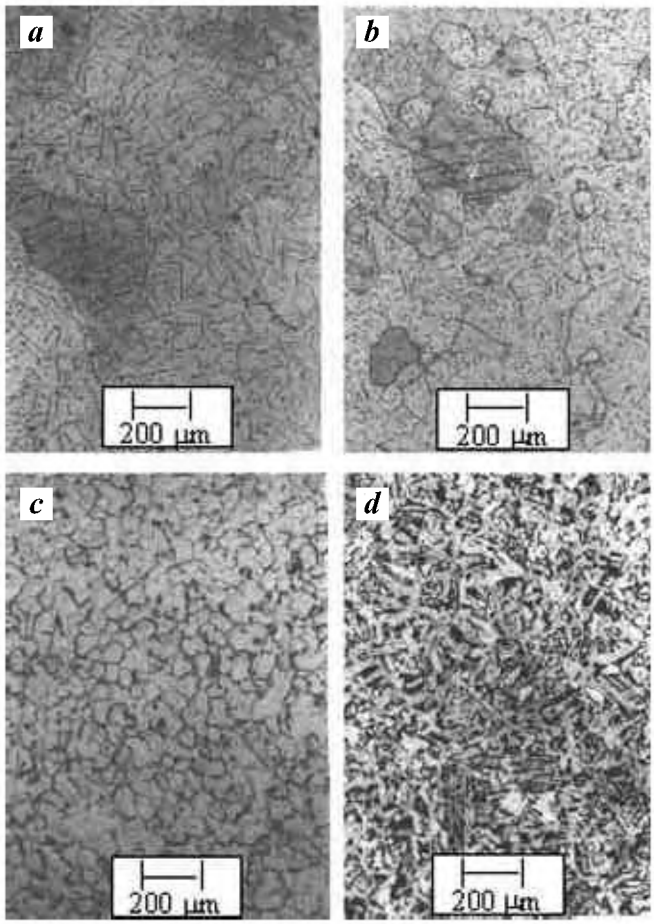

Figure 2. Microstructure of the pillar at locations (*a*) 3, (*b*) 6, (*c*) 7 and (*d*) 8 as shown in Figure 1.

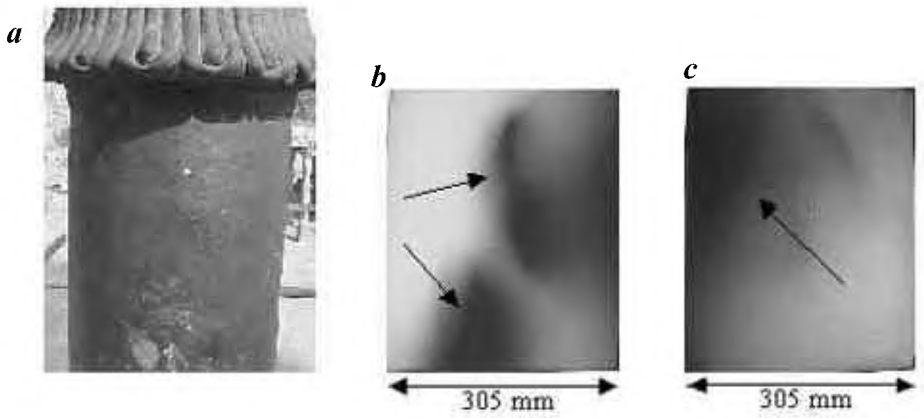

Figure 3. *a*, The top portion of the pillar. *b*, The corresponding radiograph showing presence of elongated voids detected in the top region at 0.45 m below the capital. *c*, Radiograph in a orientation 90 deg w.r.t (*b*). (Void indications are marked with arrows in the radiographs.)

The structure obtained was called 'as cast' structure as well as 'Widmanstatten' structure, and its origin was attributed to the burning or overheating of the metal above the upper critical temperature and lesser forging/metal working at those locations. These microstructures also suggest that at these places, the amount of carbon was high (> 0.2%) (ref. 5). This suggests that the microstructure obtained at the top platform possesses 'as cast' structure, however, it could also arise without melting of the metal. It has been speculated earlier that the top portion of the pillar might have been made by casting[2]. The flow lines have also been reported to be seen at the top platform of the pillar, which were attributed to the possible lightening strikes[12]. Based on this understanding, we feel that the chance of the top platform being made by cast route cannot be totally ruled out, however it requires further investigations to confirm this.

Radiography and radiation gauging were carried out on the Delhi iron pillar using isotopic Cobalt 60 source, which emits gamma rays of energy 1.17 and 1.33 MeV, that are capable of penetrating 250 mm of steel. A tungsten collimator was used to collimate the radiation beam and restrict it to the direction of interest. The entire radiography and radiation gauging campaign was carried out in night time and all safety precautions as stipulated by the Radiological Physics and Advisory Division of AERB were adhered to. For both radiography and radiation gauging the experimental configuration was identical. The source was positioned on one side of the pillar and the detector (film in the case of radiography and teletector in case of radiation gauging) was positioned diametrically opposite. Radiography was carried out in different orientations at 90° w.r.t. each other.

Radiation gauging was carried out using a teletector with telescopic handle as the detector to measure the dose levels. Radiation doses were measured diametrically opposite and also along various chord lengths. Both radiography and radiation gauging were restricted to the top region of the pillar up to a height of 1.5 m from the capital. While radiation gauging gave point information, i.e. the dose level at the point, radiography provided an image of size 15 × 12 inches. The radiation dose level was found to vary at different locations. Higher doses indicated the presence of voids, which was subsequently confirmed by radiography. The linear attenuation coefficient (μ) of γ rays was calculated and found to be in the range of 0.35 to 0.45. Within limits of experimental error, this μ value corresponds to that of iron.

Figure 3 *a* shows the photograph of the location below the capital, where radiography has been carried out. Figure 3 *b*, *c* show the typical voids detected by radiography in the same region at two different orientations at 90° w.r.t each other. A void of typically 200 mm in length with a narrow width of few mm has been observed. The second orientation (Figure 3 *c*) indicated the same void but the image was diffused indicating a very small thickness in the direction of the X-ray beam. The aspect ratio of the voids (larger dimensions in axial and circumferential directions as compared to the radial direction) indicates that the pillar could have been forged in the radial direction rather than in axial direction.

Figure 4 *a* and *b* shows the radiograph and photograph respectively of a location 1600 mm below the capital, corresponding to the cannon ball strike area. The dent is clearly seen and a triangular void is also observed below the dent. Fissures that are present in the pillar are also seen in the radiograph.

Due to the inhomogeneities present in the Delhi iron pillar, it was difficult for the higher frequencies (> 1 MHz) ultrasonic waves to penetrate in the pillar using conventional ultrasonic systems. Hence, low frequency (< 1 MHz) ultrasonic and impact echo testing have been carried out for non-destructive evaluation of the pillar. Low frequency ultrasonic technique is widely used for testing of structures having inhomogeneity and higher acoustic scattering properties. This technique uses low frequency (50 kHz–2 MHz) range and hence the attenuation of the acoustic wave is less. This makes the technique suitable for higher attenuating

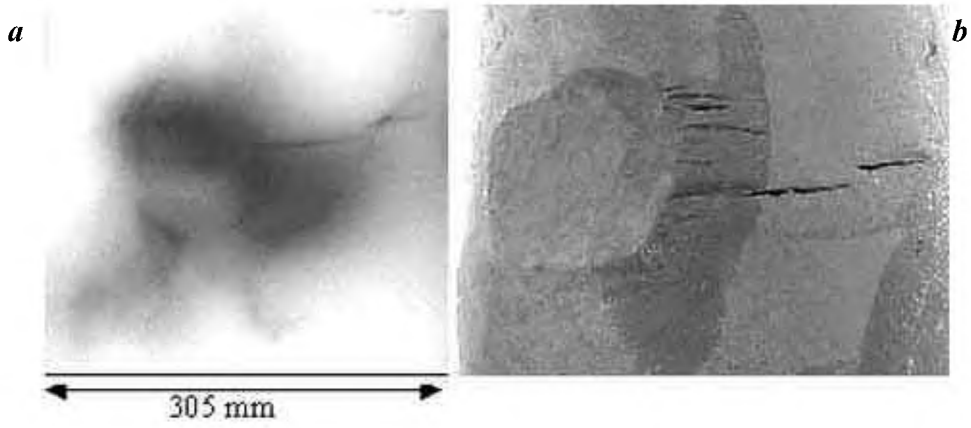

Figure 4. Radiograph with corresponding photograph at a location of 1.6 m below the capital. (cannon ball strike area).

materials. Impact echo technique was developed for testing on concrete structures due to its inhomogeneity and higher acoustic scattering properties[13]. Impact echo technique also works in low frequency (1–40 kHz) range and hence it is suitable for higher attenuating materials. This is the first time that the impact echo technique has been used for testing any metallic materials.

Low frequency ultrasonic testing has been carried out through transmission mode using a pair of 250 kHz transducers. The testing has been carried out at four different elevations using the probe fixture, especially developed for different diameters of iron pillar at different elevations. For a particular elevation, the transmitter was fixed at one location and receiver position was varied along the circumference. These measurements have been carried out to study the variation in ultrasonic velocity, and in turn the structural variation in the iron pillar. Additionally ultrasonic testing has also been carried out at every 50 mm interval in the vertical direction, covering the whole cylindrical portion of the pillar except the bottom rough portion.

The peaks corresponding to the distance between the transducers have been observed at all the elevations and at all the clock positions of the transducers, showing the transmittance of low frequency ultrasonic waves. The ultrasonic velocity has been found to be almost similar in the radial direction at all the elevations. An additional peak has been observed, after the peaks corresponding to the distance between the transducers, at some of the locations in the upper half region of the pillar. The additional peak has been found to be present in a banded region, i.e. from 0.29 to 0.54 m, 0.88–0.98 m and 1.13–1.58 m from top of the cylindrical portion of the pillar.

As this was the first time that the impact echo technique was used for testing on metallic materials, initial studies were carried out on a cylindrical steel block of diameter 280 and 620 mm height in the laboratory before applying the technique on Delhi iron pillar. Figure 5 *a* shows the impact echo signal obtained from the test block, tested diametrically. The signals obtained (Figure 5 *a*) on the cylindrical steel blocks exhibited similar trends as expected in cylindrical objects[14]. In the impact echo result, the top graph shows the as acquired time domain signal and the bottom graph the frequency spectrum of the acquired signal. The diameter of the test object, the wave speed used and the expected peak locations are given on the right side of the figures. In the impact echo testing of cylindrical bar in the radial direction, the first peak (f_1) in the frequency spectrum is expected at[14]

$$f_1 = \beta C_P/2d,$$

where C_P is the *P*-wave velocity, d is the diameter of the bar and β is a constant. As the impact echo equipment is developed for testing of concrete structures, the value of β is set as 0.92 for testing of cylindrical bars diametrically. Based on the testing on the cylindical block, the value of β for cylindrical steel specimens is determined to be 0.84 (ref. 14). Hence, the actual velocity in the cylindrical steel specimens would be 1.0952 (= 0.92/0.84) times the displayed velocity in the graph.

Impact echo testing has been carried out in grids of 250 mm height and 45° sectors, covering the whole cylindrical portion of the pillar, except the bottom rough portion. The testing has also been carried out at 50 mm interval along the vertical direction. Further, the impact echo testing has also been carried out at the decorated portion on top of the pillar. Figure 5 *b* shows the typical impact echo signal from a defect-free location of the pillar, obtained at 125 mm below the top of the cylindrical portion. By 'defect free', it is meant that the pillar is free from any defect of lateral size larger than 50 mm, in the direction of wave propagation (radial) at the point of inspection. Figure 5 *c* shows the typical impact echo signal of a defect at about 60 mm depth, obtained at 70 mm below the top of the cylindrical portion of the pillar (void detected by radiography, Figure 3 *b*).

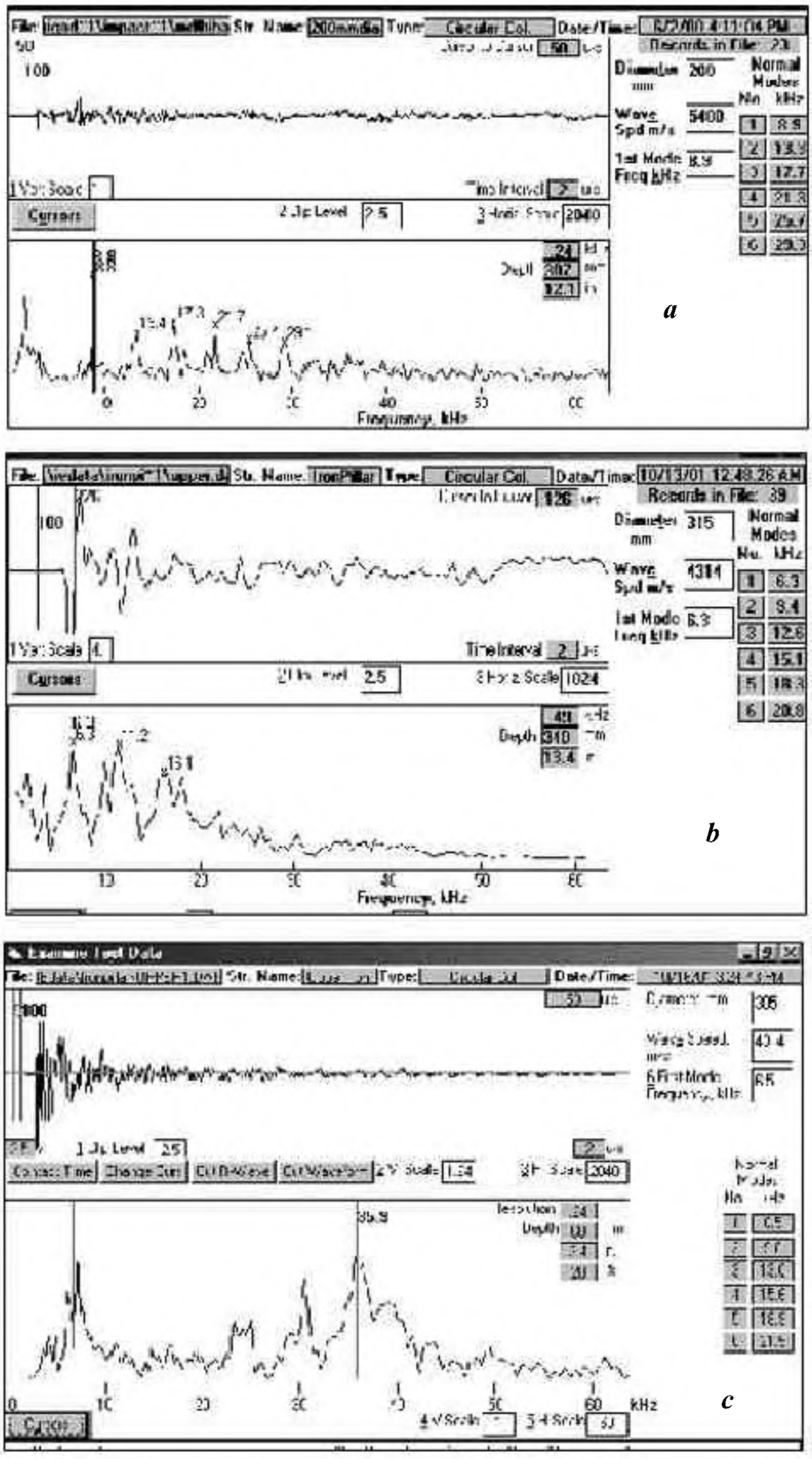

Figure 5. Typical impact echo signal from (*a*) obtained from the test block of diameter 280 mm, (*b*) a defect-free location of the pillar, obtained at 125 mm below the top of the cylindrical portion and (*c*) a defect at about 60 mm depth, obtained at 70 mm below the top of the cylindrical portion of pillar (void detected by radiography, Figure 3 *b*).

The ultrasonic velocity, as measured by impact echo testing, is found to be almost similar at all the elevations and circumferential locations in the cylindrical portion of the pillar, indicating similar structure at all elevations of the pillar. The ultrasonic velocity is found to be uniform (4675 ± 75 m/s) in the radial direction at all the elevations, indicating that the through thickness average structure (in terms of volume fraction and distribution of voids and slags) of the pillar in diametrical direction is almost uniform. It should be made clear that ultrasonic velocity is not a very sensitive function of microstructure (as compared to the accuracy in the velocity measurement using impact echo technique) in iron and carbon steels, as the maximum difference in velocity (martensite being lowest and ferrite being highest) is less than 60 m/s. Hence, any major change in the velocity can be attributed to the change in the volume fraction and distribution of the slags and voids (below the detectable limit of the technique). The decorated portion exhibited very high velocity (5325 m/s) as compared to that in the cylindrical portion. The difference in the wave velocity at these two locations is attributed to the different distributions and volume fractions of the slags as indicated by the metallographic studies (Figure 2). Further, this could also arise due to the lower volume fraction of voids in the decorative bell as compared to the main pillar. Additional peaks have also been observed and these peaks could be attributed to the presence of voids at random rather than presence of any core or planned interface. Further, the aspect ratio of the voids indicated that the pillar could have been forged in the radial direction rather than in axial direction.

X-ray fluorescence (XRF) analysis has been carried out to study variations in the chemical composition along the surface of the iron pillar. An isotope-based XRF system with hand-held probe has been used. XRF data indicated that the intensity of the iron peak was varying from region to region and also there was an increase in the background. This is attributed to the variations in the iron to other element ratio. The difference between the iron peak intensity of polished and un-polished regions was less for the main body and was more at the decorative top region. This is attributed to increase in thickness of the rust formed at the decorative top region, compared to the main body. Other elements of interest namely phosphorus, sulphur, and silicon were below the detection limits of the system.

The corrosion measurements have been carried out *in situ* at different regions of the pillar where significant changes in the appearance of the surface layers were noticed. These layers included: freshly polished surface, thin rust layer over previously polished surface, green rust layer, brown rust layer, location where *in situ* metallography was carried out a year back, and the untouched rust layer at the top of the pillar. Specially designed glass probe containing saturated silver/silver chloride electrode was attached over these regions and the corrosion potential of the surface was continuously measured using a high impedance electrometer for a period of 30 min. Anodic polarization was always initiated from well within the cathodic region for the as-polished specimens, at least about 250 mV below the corrosion potential. In the case of rusted locations, the polarization studies were started close to the corrosion potential.

The results of the present *in situ* electrochemical investigations have clearly brought out the following points with respect to understanding of the corrosion resistance of the iron pillar: (i) The as-polished surfaces at equilibrium conditions in a neutral environment are nobler than the commercially available pure iron, and that variations in the corrosion potentials at different locations indicate the heterogeneity of the surface with different microstructural conditions. This is also confirmed by the heterogeneous microstructures found at different locations of the pillar during our current investigations. (ii) Under polarization or deviation from equilibrium conditions, the commercially available pure iron showed passivation while the iron pillar corroded actively exhibiting a limiting current density, particularly of 1000 $\mu A/cm^2$ at the crown region of the capital. The high dissolution of iron from the surface with a limiting current indicated the absence of any passivation mechanism operating through the enrichment of any specific alloying element. Whether it is a cast structure, or a slag distributed structure or an annealed structure, all of them showed active dissolution. However, the rust layers formed after 10 months and 25 months on the surface of the pillar showed a tendency for passivation indicating the importance of the kinetics of corrosion reactions occurring within the 'passive' scale formed. (iii) The 'passive' rust scales formed over a long period has good stability against the transformation of oxides formed within the scale into a soluble state when a wet condition is created on the surface. The passivation current density within 14.5 to 22 $\mu A/cm^2$ for the 'passive' rust scales of the pillar formed on the surface clearly indicated the protective nature of the oxide structure developed and their stability against corrosion. The true passive behaviour of all the rusted surfaces of the pillar is a testimony for the protective nature of the scales developed over long periods. The atmospheric corrosion rate of 0.2 mils per year reported[11] by using steel samples kept at the pillar site during one year period thus would get reduced to very less values over decades of the life of the pillar. The reported thickness of the scale formed at the pillar also indicated that it varied between 50 and 500 μm considering the 1600 years of existence of the pillar[12].

The corrosion rates were calculated by using the three-point corrosion rate method using data within $\pm$ 20 mV of the corrosion potential of the polarization curves. The corrosion rates of the various conditions of as-polished and rusted scales of iron pillar, calculated from the polarisation curves are shown in Figure 6. P1 shows the corrosion rate at a location on the main body of the pillar, which was polished for *in situ* metallography 10 months before this study. P2 and P3 show the corrosion rates at 4.88 m elevation on the main pillar and crown location respectively. At these two locations, the rust was not removed earlier and hence

these locations exhibited very low corrosion rates. Similarly, P4 and P5 also show the corrosion rates at the locations on the main body of the pillar corresponding to the brown and green colours of the rust respectively. A and B show the corrosion rates of pure iron in presence of rust and in as-polished conditions respectively. P6-P11 show the corrosion rates on the pillar in as-polished conditions at base, 1.2 m elevation, 2.18 m elevation, 3.8 m elevation, 4.88 m elevation and at the crown, respectively. These results indicated that under immersed conditions of neutral electrolyte, the surface of the iron pillar corrodes at the rate of 0.395 mm per year in as-polished condition at 4.88 m elevation, whereas the corrosion rate is 0.040 mm per year in as-rusted condition at the same location. These data clearly indicate the superior corrosion resistance of the 'passive' scale of the iron pillar at a location, where it was not disturbed by any means other than the change in the atmospheric condition. The corrosion rate of 0.395 mm per year was reduced to 0.040 mm per year once a stable and 'passive' rust scale is established. However, in alternate wet and dry conditions, the kinetics of the reactions happening within the scale would significantly reduce the corrosion rate further which is why the pillar is standing without significant rusting and spalling leading to destruction, like many other iron objects of ancient times. The 'mass metal effect' and the climatic conditions of Delhi contributed significantly to the corrosion resistance of the iron pillar by providing alternate wet and dry atmospheric conditions friendly to the existence of the pillar, by helping in the stabilization of the initial 'passive' scale developed on the iron.

The present paper discusses the observations obtained through various nondestructive studies carried out on the Delhi iron pillar. For the first time, the microstructure of the ornamental portion of the pillar has been examined and reported. The microstructural analysis of the pillar indicated the presence of forged structure in the main body of the pillar, whereas a microstructure similar to 'as cast structure' is present in the top platform. Further, radiation gauging, radiography, ultrasonics and impact echo testing indicated presence of voids at different locations. No planned interface or presence of any core could be detected. The aspect ratio of the voids (larger dimensions in axial and circumferential directions as compared to the radial direction) indicates that the pillar could have been forged in the radial direction rather than in axial direction.

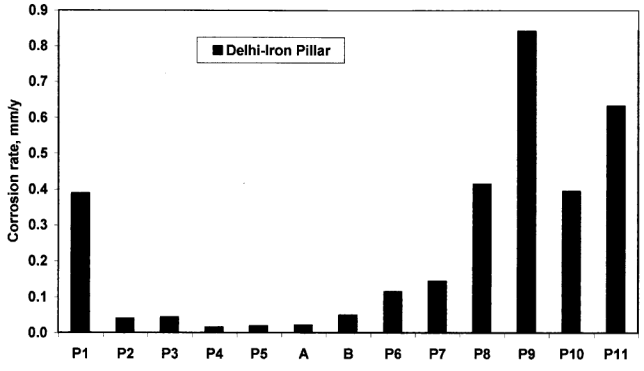

Figure 6. Corrosion rate of Delhi iron pillar at different locations and in different rust conditions. (P1 – rust, 10 months; P2 – rust, 4.88 m; P3 – rust, crown; P4 – rust, brown; P5 – rust, green; P6 – polished, base; P7 – polished, 1.2 m; P8 – polished, 2.18 m; P9 – polished, 3.8 m; P10 – polished, 4.8 m; P11 – polished, crown) (A – rust, pure iron and B – polished, pure iron).

Electrochemical investigations have brought out the following points in understanding the corrosion resistance behaviour of the iron pillar. The corrosion of as-polished surfaces at equilibrium conditions in a neutral environment is better than that of commercially available pure iron. The rust layers formed after 10 months and 25 months on the surface of the pillar show a tendency for passivation indicating importance of the kinetics of corrosion reactions occurring within the 'passive' scale formed. The 'passive' rust scales formed over a long period have good stability against transformation of oxides formed within the scale into a soluble state when a wet condition is created on the surface. Passivation current density for the 'passive' rust scales of the pillar formed on the surface indicate the protective nature of the oxide structure developed and its stability against corrosion.

The present study has brought out interesting and important insights related to internal defects, microstructure and fabrication methodology of the Delhi iron pillar. However, further studies are required for comprehensive characterization of the pillar and to understand its corrosion behaviour in depth. Hardness measurements at various locations on the pillar may bring out chemical and structural inhomogeneities in the pillar and systematic variation in the property, if any. Real time radiography and tomography using LINAC may be useful for complete characterization of the internal structure of the pillar. Ultrasonic studies at higher frequencies (2–5 MHz) with high energy will lead to better resolution in defect characterization and this can also be extended for the ultrasonic imaging using synthetic aperture focusing technique (SAFT). Further metallographic, XRD and other dating studies are required for an estimation of the era of fabrication of decorative portion of the pillar as compared to its main body. Periodic XRF studies on the polished region of the pillar may provide the kinetics and mechanistic aspect of the corrosion resistance of the pillar. Further, the true date of 'passive' rust scale needs to be analysed by nuclear techniques, as it is an important parameter to consider in proposing a model and mechanism by which the corrosion of the pillar withstood alternate wet and dry conditions over 1600 years.

1. Anantharaman, T. R., *The Rustless Wonder – A Study of the Delhi Iron Pillar*, Vigyan Prashar, New Delhi, 1997.
2. Rao, K. N. P., *Met. News*, 1991, **13**, 9–15.
3. Sir Rodert Hadfield, *J. Br. Iron Steel Inst.*, 1912, **85**, 134.
4. Lal, B. B., in *The Delhi Iron Pillar: Its Art, Metallurgy and Inscriptions* (eds Joshi, M. C., Gupta, S. K. and Goyal Shankar), Kusumanjali Book World, Jodhpur, 1996, pp. 22–58.

5. Lahiri, A. K., Banerjee, T. and Nijawan, B. R., *NML Tech. J.*, 1963, **5**, 46.
6. Bindal, V. N., Ashok Kumar, Som, J. N., Chandra, S., Yudhisther Kumar and Lal, J., Ultrasonic International 89, Conference Proceedings, Madrid, July 1989, pp. 95–100.
7. Bardgett, W. E. and Stanners, J. F., *J. Iron Steel Inst.*, 1963, 3–10.
8. Ghosh, M. K., *NML Tech. J.*, 1963, **5**, 31–45.
9. Wagner, C. and Traud, W., *Z. Elektrochemie*, 1938, **44**, 391.
10. Balasubramaniam, R., *Trans. Indian Inst. Met.*, 1997, **50**, 23.
11. Balasubramaniam, R., *Delhi Iron Pillar: New Insights*, Aryan Books International, New Delhi, 2002.
12. Balasubramanian, R., *Curr. Sci.*, 2003, **84**, 534–541.
13. Sansalone, M., *ACI Struct. J.*, 1997, **94**, 777.
14. Anish Kumar, Rajkumar, K. V., Jayakumar, T., Kalyanasundaram, P. and Baldev Raj, Impact echo testing of Delhi iron pillar. *NDTE Int.*, 2004 (Commun.)
15. Hudson, J. C., *Nature*, 1953, **172**, 499.
16. Wranglen, G., *Corros. Sci.*, 1970, **10**, 761.

ACKNOWLEDGEMENTS. We thank the Department of Science and Techonology and Archeological Society of India for their support for studies on the Delhi iron pillar. We also thank Dr S. L. Mannan, Associate Director, Materials Development Group for useful discussions.

Received 16 January 2004; revised accepted 5 February 2005

RAPD markers for genetic diversity study among Indian cotton cultivars

M. K. Rana* and K. V. Bhat

National Research Centre on DNA Fingerprinting,
National Bureau of Plant Genetic Resources, Pusa Campus,
New Delhi 110 012, India

The present study was undertaken with RAPD markers for genetic diversity estimation in 59 cotton cultivars belonging to four cultivated species of cotton. The selected eighteen RAPD primers produced a total of 251 amplicons, which generated 97.21% polymorphism. The number of amplification products ranged from 7 to 24 for different primers, whereas per cent genetic similarity for the studied primers ranged from 42 to 79. Among 59 cotton cultivars, 36% genetic diversity was observed. In 41 *Gossypium hirsutum* cultivars included in the study, the average genetic similarity was 74%. More genetic diversity was observed in diploid than in tetraploid cotton cultivars. UPGMA cluster analysis placed tetraploid cotton cultivars into two distinct clusters that are in agreement with the traditional taxonomic arrangement of these cultivars into *G. hirsutum* and *G. barbadense*. Analysis of molecular variance in *G. hirsutum* cultivars revealed that most of the variance could be attributed to within breeding-centre variance. All the cultivars could be discriminated from one another based on the combined profiles for eighteen oligonucleotide primers. A negative correlation between average genetic similarity for a primer and the number of cultivars identified by it was observed. Genetically distinct cultivars were identified that could be potentially important sources of germplasm for further cotton improvement in the country.

*For correspondence. (e-mail: mkrana@nbpgr.delhi.nic.in)

THE genus *Gossypium* to which cultivated cottons belong, contains about 45 diploid ($2n = 2x = 26$) and five allotetraploid ($2n = 4x = 52$) species[1], all of which are basically tropical perennials. Two of the diploids, *G. arboreum* L. and *G. herbaceum* L. and two of the allotetraploids, *G. hirsutum* L. and *G. barbadense* L. are cultivated as annuals for their seed and fibre in the tropical and subtropical regions of the world. The allotetraploids are the most commonly grown, making up more than 90% of the world production. Cotton is an important cash crop of India. About 60 million people earn their livelihood through its cultivation or trade and processing. The present lint yield[2] in the country is 308 kg/ha, which was only 151 kg/ha during 1970. All the four cultivated species of cotton grown around the world are grown in India.

Recently, various molecular marker techniques have developed into powerful tools for diversity analysis and establishing relationships between cultivars. Among these, the RAPD technique[3,4] is technically the simplest, less expensive, fast and does not require huge infrastructure to start with.

The RAPD technique has already been used in cotton for genetic diversity studies. In nine Australian cotton cultivars belonging to *G. hirsutum*, 92.1 to 98.9% genetic similarity was observed using this technique[5]. Again, using RAPD markers and morphological traits, the genetic relatedness in 16 elite cotton genotypes was studied and a positive correlation ($r = 0.63$) between the genetic distances derived based on molecular markers and the taxonomic distances calculated on the basis of morphological markers was observed[6]. In yet another study[7] involving 22 *G. hirsutum* varieties, 89.1% polymorphism was observed. Seventeen varieties that could be placed in one cluster had a similarity range of 81.5–93.4%. The only diploid cultivar in this study shared 55.7% genetic similarity with tetraploid counterparts. In diploid cottons belonging to *G. arboreum* and *G. herbaceum* 72% genetic similarity has been reported[8]. Besides these diversity studies, the RAPD technique has also been used for phylogeny[9] and seed purity studies[10] in cotton. Thus the usefulness of this technique for diversity studies and establishing genetic relationships is well documented in cotton.

The experimental material in the present study consisted of fifty-nine cultivars of cotton belonging to four cultivated species (Table 1). These included 11 intra- or inter-specific hybrids that will be referred to as cultivars hereafter. Excluding hybrids, 33 cultivars belong to *G. hirsutum*, whereas five each belong to the three species *G. barbadense*, *G. arboreum* and *G. herbaceum*. These cultivars were pro-